SURFACE MAPPING OF SELECTED REGIONS IN THE ORION NEBULA

P. M. Perry, B. E. Turnrose, C. A. Harvel,
R. W. Thompson, A. D. Mallama

Computer Sciences Corporation
Astronomy Department

ABSTRACT

Low-dispersion, large-aperture, ultraviolet spectra ($\lambda\lambda$ 1135-3255Å) of selected regions in the Orion Nebula were obtained with the International Ultraviolet Explorer (IUE) scientific instrument. Spectra obtained at 35 contiguous locations defining a mosaic within the nebula were used to generate monochromatic images of high spatial resolution at the wavelengths of the ultraviolet emission lines CIII] λ1909, CII] λ2326, and [OII] λ2470. Image-processing techniques were utilized to generate and analyze these ultraviolet surface maps. The imagery at the three wavelengths studied shows definite differences in the spatial distribution of emission from the CII] CIII] and [OII] ions. Ways of using the imagery to determine ionization structure and C/O abundance ratios throughout the regions observed are being developed, in addition to means of analyzing the extensive continuum measurements in terms of dust-scattering characteristics.

INTRODUCTION

The central (Huygenian) region of the Orion Nebula (NGC 1976) possesses a wealth of fine structural detail which can only be studied with high-resolution instruments. Many studies have been carried out on visual images of the central region but, until recently, it was not feasible to obtain images of sufficiently high resolution in the far UV. Existing UV imagery (e.g., ref. 1), although of considerable scientific value, displays only large-scale surface detail.

The launching of the IUE has provided a unique opportunity to extend the high-resolution study of the surface features of the Orion nebula into the far UV. Even though the IUE scientific instrument described by ref. 2 is primarily designed to operate as a conventional spectrograph, its high degree of attitude stability and pointing accuracy, together with an extended sky coverage (10 by 20 arcseconds) using the large entrance aperture, give it the capability--when used in the mode to be presently described --of obtaining high spatial resolution images in the far UV. The observational technique involves the acquisition of low-dispersion spectra through the large aperture in both the long- and short-wavelength spectrographs. Contiguous image segments, defined by the size of the aperture, are obtained in a raster pattern covering the program area. As in a slitless spectrograph, each image segment is simultaneously accumulated at all wavelengths. The image processing operations to be described then reconstruct monochromatic images of the nebula in the wavelengths of the UV emission lines from a mosaic of the individual segments.

The following section of this paper describes the specific observational procedure used to obtain the images. The next section details the processing techniques employed in obtaining a preliminary set of "raw" mosaics, and then describes methods to be employed to further remove instrumental signature and improve the image reconstruction integrity. These raw mosaics are presented in the last section which contains a preliminary discussion of their significance and the use of the data obtained by this program in several scientific areas.

OBSERVATIONS

During the period from April 23 to April 28, 1979, a series of 69 large-aperture, low-dispersion images were taken covering a total of 35 contiguous overlapping areas in the central (Huygenian) region of the nebula. This area extends from just south of θ^2Ori A in a northwesterly direction across the bright bar towards θ^1Ori C (see Figures 1 and 2, and Table I). For all but one of these areas, both a long- and a short-wavelength camera exposure were obtained.

Figures 1 and 2 and Table I define the 35 areas used to form the mosaic and locate the mosaic as a whole within the nebula. Figure 1 shows the contiguous area observed outlined on a visual photograph of the central part of the nebula. Figure 2 shows the placement, orientation, and extent of each of the 35 areas observed; Table I gives the RA and DEC of each area, as well as the image number of the observation with each camera and the exposure time used. At the time of these observations, the spacecraft was oriented such that the long axis of the large aperture ran very nearly north-south.

As can be seen in Table I, exposure times for LWR and SWP were about 15 and 10 minutes, respectively. When possible, the exposure time for an area was estimated from the exposure time and exposure level of previously observed adjacent areas. In one case (area 32), the position of the area was changed to move it away from a bright star (θ^2A) after an adjacent area (area 33) was saturated by scattered light from the star.

Pointing of the spacecraft was maintained to an accuracy of 3 arcseconds or better (this is less than the spatial resolution of the system) by setting on θ^2Ori C (assumed 1950.0 coordinates: RA = $5^h33^m\ 04.^s0$, DEC = $-5^\circ27'\ 09".0$), offsetting to the RA and DEC of the target area, and then quickly acquiring θ^2Ori C as a guide star. The spacecraft gyros were trimmed to minimize drift during the maneuver. In those cases where an observation of the same area was immediately made using the other camera, the spacecraft was maneuvered to place the area in the large aperture of the other camera without going back to the set star. After each observation or set (LWR, SWP) of observations, the spacecraft was offset back to θ^2Ori C using the inverse of the offsets used to get to the target area. The difference between the expected FES location of the set star and its actual location was obtained in order to estimate the combined offset and drift error during the observation--this error was less than 3 arcseconds in all cases and usually around 1.5 arcseconds.

PROCESSING TECHNIQUES

The 35 observations described in the preceding section were first processed in the standard fashion at the IUE Image Processing Center (ref. 3). An example of a raw LWR image of the nebula is given in Figure 3, which illustrates the appearance of the CII]λ2326 and [OII]λ2470 lines against the continuum radiation. Each observation yields a two-dimensional array of fluxes arranged by wavelength and spatial position perpendicular to dispersion; this is the so-called line-by-line or spatially resolved spectrum which is used herein as the starting point for our special processing. Since the imagery to be reconstructed here is monochromatic, the wavelength dimension also translates into position; i.e., there is spatial resolution along the dispersion direction. Thus, from the line-by-line spectra of each observation, we can derive a two-dimensional image segment of that portion of the nebula subtended by the large aperture, for each of the UV emission lines observed. The purpose of our tailored processing is to assemble these segments into a set of monochromatic mosaics of the nebula, and to remove residual instrumental effects as well as any effects due to the particulars of the observations. For each of the mosaics, the following procedures are used.

A data array is dimensioned (51 x 69) to cover the program region (Figures 1 and 2) with a basic resolution of one IUE line-by-line spectrum sample. The celestial coordinates of the observations are read from the IUE image header, verified with handkept observing logs, and converted to the corresponding relative coordinates of our data matrix. At the same time, the exposure time is read from the IUE header and stored in core for later use.

The wavelengths in the line-by-line spectra are then read, and the locations of the emission lines of interest and suitable continuum background regions are noted. Then the fluxes are read from the appropriate locations. The image segment derived from this data is 5 line-by-line samples wide in the dispersion direction and 11 line-by-line samples high in the perpendicular direction. This corresponds closely to the 10 x 20 arcsecond dimensions of IUE's large aperture. (Remember that each line-by-line sample is $\sqrt{2}$ IUE pixels, or 2.16 arcseconds, on a side). Next, the background fluxes are interpolated within each line-by-line pseudo order and subtracted from the emission line fluxes. The resulting data are then normalized to a constant exposure time. The normalized fluxes are added to the data matrix, and an increment is added to the corresponding elements of a counter matrix.

When all the data have been so processed, the data matrix is divided by the counter matrix (in order to properly average the fluxes in grid elements where the observations were overlapped). Then the data are normalized to a maximum value of 30,000 for use by a COMTAL display device*, a header is added, and the resulting file is copied to tape.

The procedures described above result in preliminary mosaic imagery. Ways of further correcting and improving such data are currently under development. The effective transmission function, or vignetting function, for each element within the large aperture is being measured on unsaturated exposures of the geocoronal Lyman alpha line. SWP mosaics will be corrected for this function, and the possibility of relating that correction to LWR data will be

*Provided by the Laboratory for Astronomy and Solar Physics, GSFC.

investigated. Also, the possibility of using bilinear interpolation to render a more exact correspondence between the placement of the large aperture and the derived grid elements is being studied.

DISCUSSION

Figure 4 compares a visual image of the program region of the Orion nebula with the three preliminary UV mosaics which have been generated from the present data, using the emission lines CIII] λ 1909 (SWP), CII] λ 2326 (LWR), and [OII] λ 2470 (LWR). Note that the bright filamentary bar identified with an ionization front is visible in all three mosaics. The emission line from the singly ionized species (CII] and [OII]) is concentrated near the ionization front, whereas the emission from doubly ionized carbon is spread more throughout the principal HII region. The bar in the [OII] imagery appears to show a region of diminished intensity near the western end. In both CII] and [OII] there is detectable emission south of the bar, including fairly strong emission in the isolated region (to the east of the principal program area) which includes the compact optical object referred to as "cloudlet C" by Táylor and Münch (ref. 5). The cloudlet is a relatively low excitation object since no CIII] emission is seen. The general lack of CIII] emission south of the bar is another feature evident from the preliminary mosaic, even though the CIII imagery has the lowest signal-to-noise ratio because of the faintness of the λ1909 emission. Since that line is even weaker in the LWR spectra, only SWP spectra were used in generating the λ1909 mosaic. The SWP fluxes were corrected for ITF error using the Three Agency correction algorithm SWPFIX (ref. 4).

The data as they now stand indicate that several promising avenues of research are feasible. The imagery will be calibrated absolutely to obtain emission line intensities as a function of position with a resolution of about 4-5 arcseconds. Such intensity maps, perhaps corrected for density fluctuations by dividing through by an Hα image*, will be used to compare the ionization structure measured by the spatial distribution of the CII], CIII], and [OII] UV emission to the results of optical studies. The preliminary UV results compare favorably with optical measurements indicating that the higher ionization states are found chiefly within the principal inner HII region (see, for example, ref. 6). These data may also be compared to the less extensive UV measurements of Torres-Peimbert, et al. (ref. 7), and Bohlin, et al. (ref. 8). In particular, the present data will be used according to the considerations of refs. 7, 8, and 9 to measure the C/O abundance ratio as a function of position and compare it to the earlier results which find either solar values (ref. 7) or twice solar values (ref. 8) for C/O in Orion.

The measurements of the nebular continuum which are accumulated in the present program at all wavelengths from λ1150 Å to 3200 Å are of considerable interest in their own right in characterizing the properties of dust scattering as a function of position in the nebula. The grid of continuum measurements obtained here will ultimately be presented in a form suitable for dust studies. In this regard, we intend particularly to map the strength of the 2200 Å extinction feature in the bar, cloudlet C, and two other Taylor-Münch cloudlets (ref. 5) also observed.

*R. J. Dufour, private communication (1980)

REFERENCES

1. Carruthers, G. R., and Opal, C.: Ap.J, vol. 217, 1977, p. 95.

2. Boggess, A., et al., The IUE Spacecraft and Instrumentation, Nature, vol. 275, Oct. 1978, p. 2.

3. Klinglesmith, D. A., Perry, P. M., and Turnrose, B. E.: The International Ultraviolet Explorer Spectral Image Processing System, Proceedings of the Society of Photo-Optical Instrumentation Engineers, vol. 172, 1979, p. 279.

4. Cassatella, A., et al., A Correction Algorithm for Low Disperson SWP Spectra, NASA IUE Newsletter No. 8, 1979.

5. Taylor, K., and Münch, G.: Astron. Astrophys., vol. 70, 1978, p. 359.

6. Balick, B., Gammon, R. H., and Hjellming, R. M.: Pub. A.S.P., vol. 86, 1974, p. 616.

7. Torres-Peimbert, S., Peimbert, M., and Daltabuit, E.: IUE and Visual Observations of the Orion Nebula and IC 418: The Carbon Abundance (preprint), 1979.

8. Bohlin, R. D., Hill, J. K., Stecher, T. P., and Witt, A. N.: Long-Slit Spectroscopy in the Rocket Ultraviolet of the Orion Nebula, Ap. J. (in press).

9. Dufour, R. J., Talbot, R. J., Jr., and Shields, G. A.: The Carbon Abundance in Two HII Regions of the Small Magellanic Cloud. The Universe in Ultraviolet Wavelengths: The First Two Years of IUE. NASA CP 2171, 1980: this compilation.

TABLE I - LOG OF OBSERVATIONS

	RA			DEC			SWP		LWR	
AREA#	h	m	s	deg	m	s	IMAGE#	EXP*	IMAGE#	EXP*
1	5	32	50.87	-5	25	28.0	5068	10.0	4401	15.0
2			51.40			28.0	5061	10.0	4394	11.25
3			51.93			28.0	5053	10.0	4386	15.0
4			51.13			44.0	5069	10.0		
5			51.67			44.0	5060	10.0	4393	15.0
6			52.20			44.0	5052	10.0	4385	15.0
7			52.73			44.0	5065	10.0	4398	15.0
8			51.93		26	00.0	5059	10.0	4392	15.0
9			52.47			00.0	4997	8.0	4334	12.0
10			53.00			00.0	5051	10.0	4384	15.0
11			53.53			00.0	5050	10.0	4383	15.0
12			52.20			16.0	5058	10.0	4391	15.0
13			52.73			16.0	5054	10.0	4387	15.0
14			53.27			16.0	5036	10.0	4364	15.0
15			53.80			16.0	5034	10.0	4362	15.0
16			54.33			16.0	5066	10.0	4399	15.0
17			54.87			16.0	5067	10.0	4400	15.0
18			52.47			32.0	5057	10.0	4390	15.0
19			53.00			32.0	5055	10.0	4388	15.0
20			53.53			32.0	5035	10.0	4363	15.0
21			54.07			32.0	5033	8.0	4361	12.0
22			54.60			32.0	4996	8.0	4333	12.0
23			56.73			29.0	5049	9.0	4359	12.0
24			52.73			48.0	5056	10.0	4389	15.0
25			53.27			48.0	5032	8.0	4360	12.0
26			53.80			48.0	5031	8.0	4344	9.0
27			54.33			48.0	5000	8.0	4336	12.0
28			54.87			48.0	4999	2.0	4335	2.5
29			52.47		27	04.0	not observed			
30			54.07			04.0	5007	8.0	4342	12.0
31			54.60			04.0	5003	8.0	4339	12.0
32			55.13			09.0	5002	6.0	4338	9.0
33			55.67			04.0	5001	2.0	4337	3.0
34			54.87			15.0	5006	10.0	4342	15.0
35			55.40			20.0	5005	8.0	4341	15.0
36			55.93			20.0	5004	6.0	4340	9.0

*All exposures given in minutes.

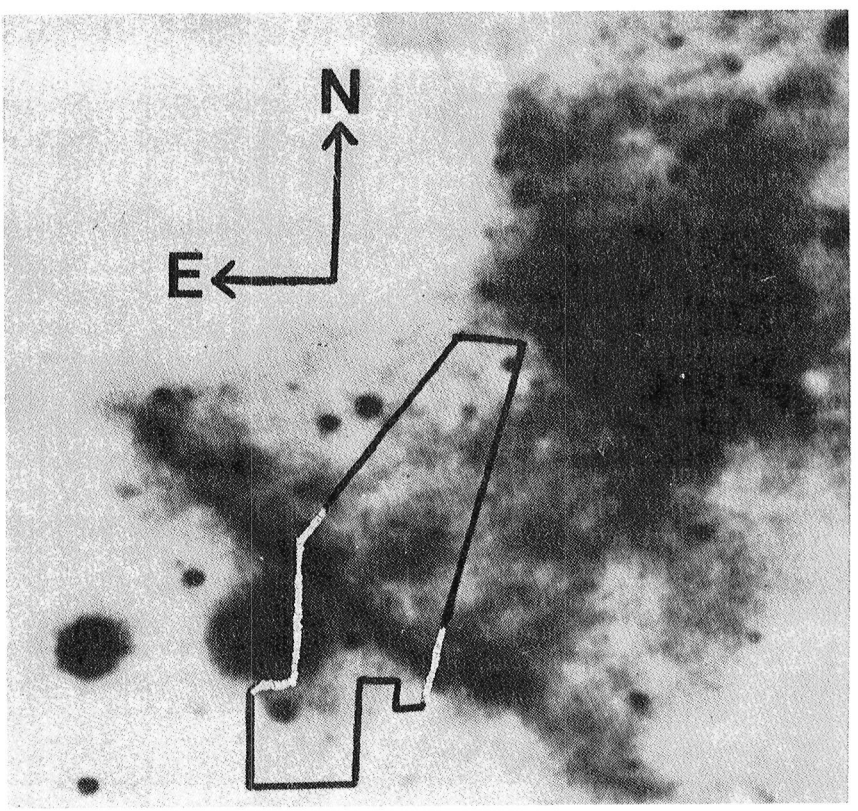

Figure 1 — [OI]λ6300 photograph of the central region of the Orion Nebula (courtesy T. R. Gull, GSFC) with UV survey area outlined.

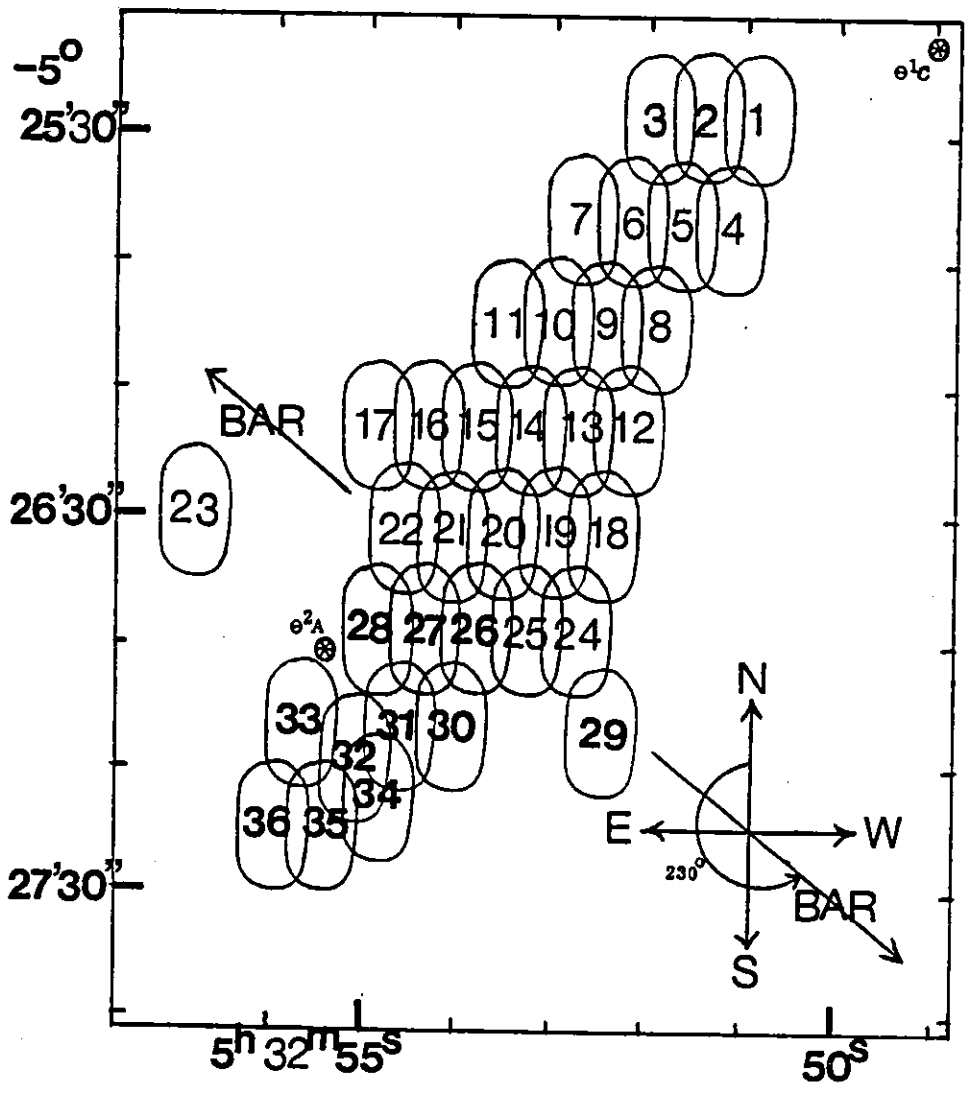

Figure 2 — Schematic drawing showing placement and orientation of survey apertures.

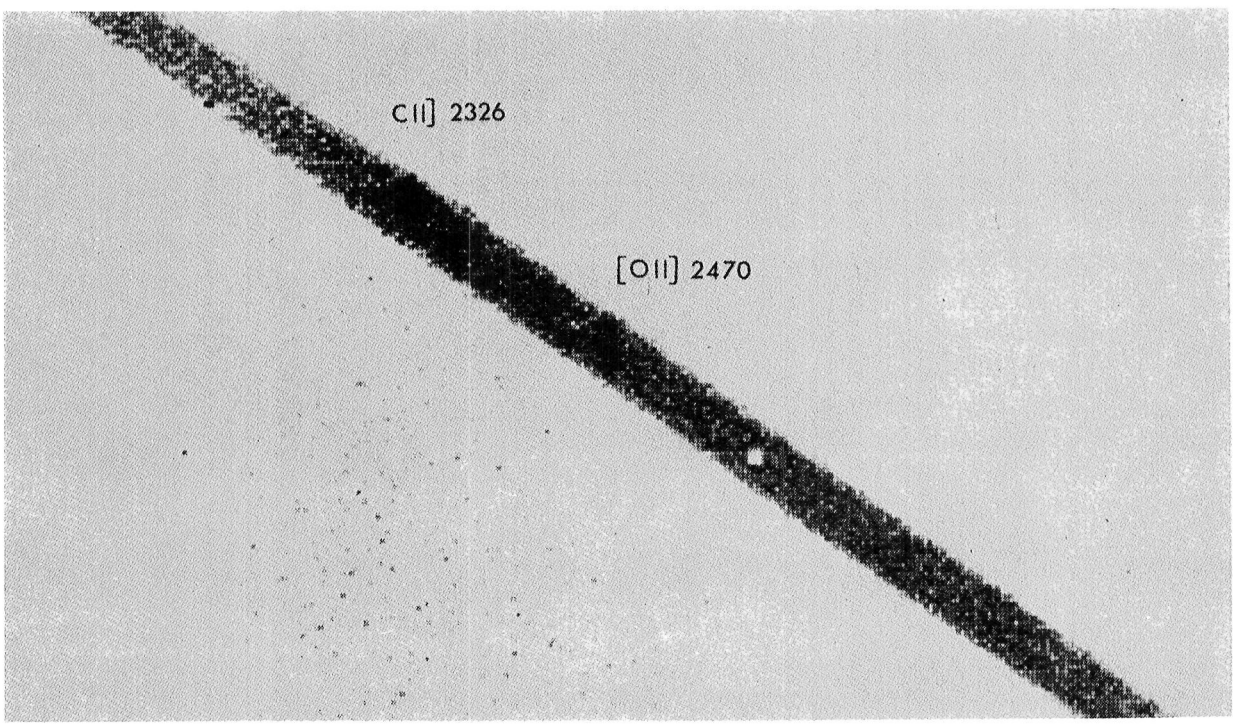

Figure 3 — Enlargement of raw image (LWR 4389, area 24) showing the CII] λ2326 and [OII]λ2470 emission lines against the continuum radiation.

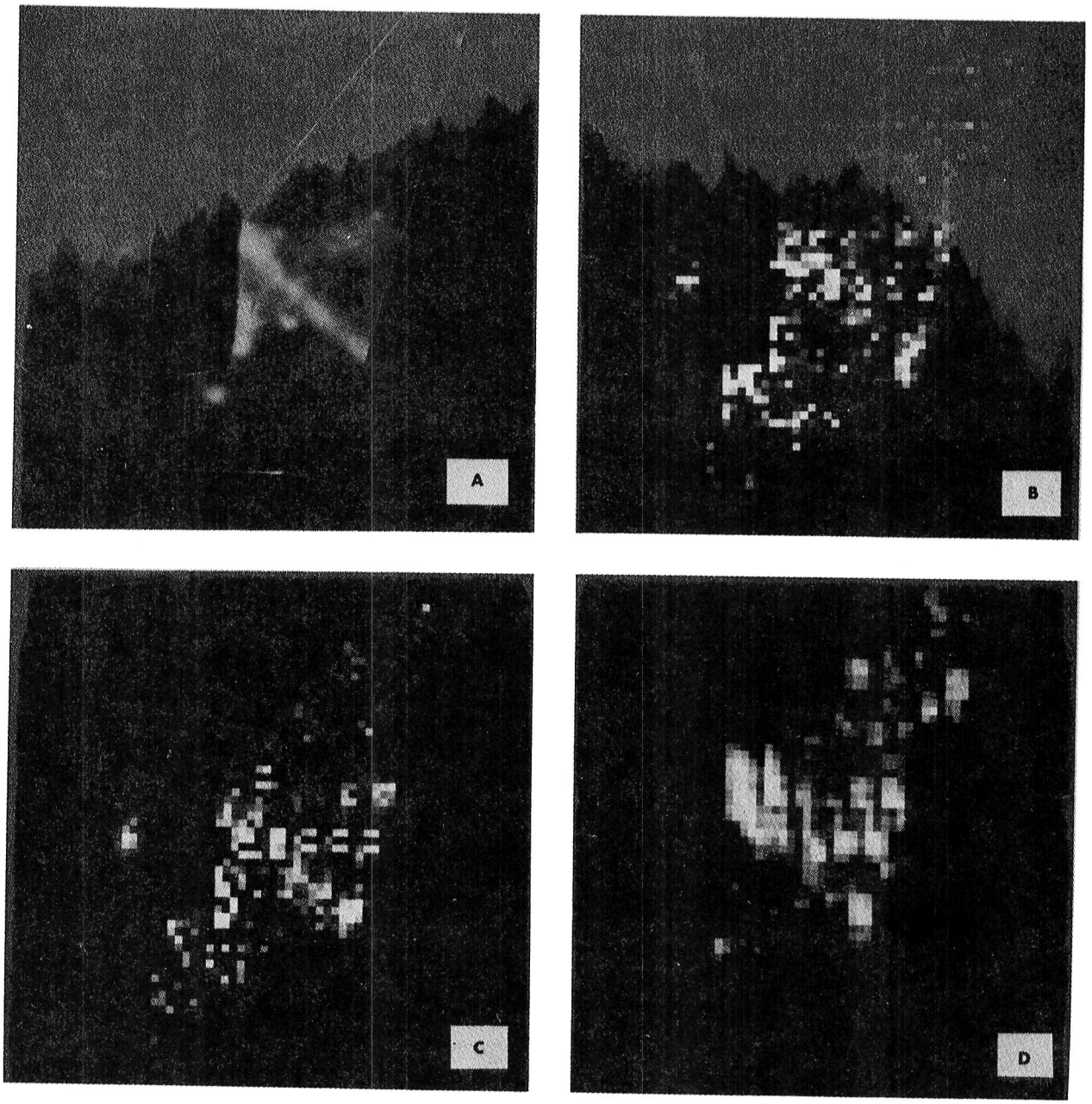

Figure 4 — Comparison of survey region in visual and UV wavelengths:

a. [OI]λ6300

b. [OII]λ2470

c. CII]λ2326

d. CIII]λ1909

Note that the brightness of each UV mosaic is scaled so that the highest intensity in that mosaic is white and zero or negative intensity is black. Relative intensities between the three mosaics cannot be inferred from these photographs.